Available online at www.sciencedirect.com
ScienceDirect
Catalysis Today 123 (2007) 208–217
CATALYSIS TODAY
www.elsevier.com/locate/cattod

Preparation and characterization of inexpensive heterogeneous catalysts for air pollution control: Two case studies

Shigenori Utsumi [a], Fernando E. Vallejos-Burgos [a], Claudia M. Campos [b], Ximena García [a], Alfredo L. Gordon [a], Gina Pecchi [b,*], Ljubisa R. Radovic [a,c,**]

[a] *Department of Chemical Engineering, University of Concepción, Concepción, Chile*
[b] *Department of Physical Chemistry, University of Concepción, Concepción, Chile*
[c] *Department of Energy and Geo-Environmental Engineering, The Pennsylvania State University, University Park, PA 16802, USA*

Available online 17 January 2007

Abstract

Relatively inexpensive heterogeneous catalysts for two reactions of great importance in air pollution control, NO reduction and VOC combustion, were prepared and characterized. Apart from their common practical goal and the frequent need for simultaneous removal of air pollutants, these reactions share a similar redox mechanism, in which the formulation of more effective catalysts requires an enhancement of oxygen transfer.

For NO reduction, supported catalysts were prepared by adding a metal (Cu, Co, K) using ion exchange (IE) and incipient wetness impregnation (IWI) to chars obtained from pyrolysis of a subbituminous coal. The effects of pyrolysis temperature, between 550 and 1000 °C, on selected catalyst characteristics (e.g., BET surface area, XRD spectrum, support reactivity in O_2) are reported. For IE catalysts, the surface area increased in the presence of the metals while the opposite occurred for IWI catalysts. For the Co-IE catalysts, the highest surface area was obtained at 700 °C. The XRD results showed that, except for Cu (which exhibited sharp Cu^0 peaks), the catalysts may be highly dispersed (or amorphous) on the carbon surface. For the C–O_2 reaction the order of (re)activity was K ≫ Co > Cu for IE catalysts and K > Cu > Co for IWI catalysts. For NO reduction the orders were K > Co > Cu (IE catalysts) and Cu > Co > K (IWI catalysts). In all cases the catalytic (re)activity for NO reduction was lower than that exhibited for the C–O_2 reaction. The K-IE and Cu-IWI catalysts appeared to be the most promising ones, although further improvements in catalytic activity will be desirable. Some surprising results regarding CO and CO_2 selectivity are also reported, especially for Co catalysts.

In VOC combustion, the effect of the nature of ion B (Fe and Ni) on the partial substitution of ion A (Ca for La) in ABO_3 perovskites (e.g., $LaFeO_3$ and $LaNiO_3$) and on their catalytic activity was studied. The perovskite-type oxides were characterized by means of surface area measurements, XRD, temperature-programmed desorption (TPD) and temperature-programmed reduction (TPR). The effect of partial substitution of La^{3+} by Ca^{2+} was more significant for the $La_{1-x}Ca_xFeO_3$ perovskites. In this case, the electronic perturbation is compensated by an oxidation state increase of part of Fe^{3+} to Fe^{4+}. The TPD results revealed that, at higher substitution levels, oxygen vacancies are also formed to preserve electroneutrality. For the $La_{1-x}Ca_xNiO_3$ perovskites, the characterization results showed no evidence of large differences in electronic properties as calcium substitution increases. The $La_{1-x}Ca_xNiO_3$ perovskites exhibited lower activity than the simple $LaNiO_3$ perovskite, whereas for the $La_{1-x}Ca_xFeO_3$ substituted perovskites the most active catalyst (exhibiting the lowest ignition temperature) was obtained at the highest substitution level, $La_{0.6}Ca_{0.4}FeO_3$.

The performance of both groups of catalysts is briefly discussed in terms of redox processes, in which the interplay between oxygen transfer and electron transfer requires further elucidation for the improvement of catalytic activity.

Keywords: Heterogeneous catalysts; Perovskite; Ion exchange; Incipient wetness impregnation; Redox mechanism; Carbon support

1. Introduction

Air pollution control is a pressing need in both industrialized and developing nations. The introduction of effective catalytic processes for pollutant destruction is often hampered in developing nations by excessive emphasis on economic

* Corresponding author.
** Corresponding author at: Department of Energy and Geo-Environmental Engineering, The Pennsylvania State University, University Park, PA 16802, USA.
E-mail addresses: gpecchi@udec.cl (G. Pecchi), lrr3@psu.edu (L.R. Radovic).

0920-5861/$ – see front matter © 2007 Elsevier B.V. All rights reserved.
doi:10.1016/j.cattod.2007.01.009

development, at the expense of environmental protection. The affordability of any newly developed catalyst or catalytic process is thus a critical issue, which we have addressed in the following manner: (a) use of coal instead of activated carbon as a precursor for carbon-supported catalysts for NOx control; (b) use of perovskites prepared from metal nitrates instead of supported noble metals for destruction of volatile organic compounds (VOC).

Carbon has been a popular catalyst support for many years [1]. In some liquid-phase applications it is irreplaceable, because of its tolerance of both highly acidic and highly basic solutions. And yet the virtues and the flexibility of carbon supports have not been exploited to their fullest extent, mostly because of a lack of appreciation of the potentially widely varying surface chemistry of carbon materials [1,2]. Another challenge is related to the ease of reproducible preparation and the cost of carbon-supported catalysts. We have recently initiated a research program that is meant to address both these issues, using inexpensive and abundant coal and biomass as precursors to carbon supports for several representative catalysts: potassium, copper and cobalt. As test reactions we selected H_2O_2 decomposition and NO reduction or decomposition, in which carbon can best exhibit its remarkable flexibility, not only as a support but also as a catalyst in its own right as well as a reducing agent. In addition to the practical importance of each one of these two reactions – the former is a key electron transfer step for the efficient use of batteries and fuel cells [3] and the latter is the key to effectively combating smog and acid rain – they are expected to share a crucial mechanistic feature, as summarized in the following reaction sequence:

$$2C_f + 2NO \rightarrow N_2 + 2C(O) \quad (1)$$

$$C_f + H_2O_2 \rightarrow C{-}O + H_2O \quad (2)$$

$$C(O) \leftrightarrow C{-}O \quad (3)$$

$$2C{-}O \rightarrow O_2 + 2C_f \quad (4)$$

$$2C(O) \rightarrow CO_2 + C_f \quad (5)$$

The reduction of NO (reactions (1), (3) and (5)) on the free carbon active sites (C_f) is known to follow the same general (''oxygen transfer'') mechanism as both catalyzed and uncatalyzed carbon combustion or gasification [4]: the reactive intermediate (C(O)) is either in (temporary) equilibrium with the stable complex (C–O) or decomposes to CO_2 (at relatively low temperature, e.g., <500 °C; at higher temperatures CO is produced as well). In the often more desirable decomposition of NO (reactions (1), (3) and (4)), carbon acts as a true catalyst, and not also as a reducing agent. This is also a unique feature of H_2O_2 decomposition (reactions (2) and (4)). The proposed mechanism highlights the critical importance of the surface chemistry of carbon, which in turn depends on both its pyrolysis (or heat treatment) conditions and the nature of its precursor [5,6]: the relative abundance of C(O) versus C–O surface species (e.g., at the edges of carbon crystallites and within the graphene layers, respectively) is expected to govern both carbon (re)activity and product selectivity. In the presence of an active metal catalyst (M) on the carbon support [5,7], the complementary reactions are the more effective adsorption of oxygen from NO or H_2O_2,

$$2M + 2NO \rightarrow N_2 + 2M(O) \quad (6)$$

$$M + H_2O_2 \rightarrow H_2O + M(O) \quad (7)$$

and the transfer ('spillover') of surface oxygen from the catalyst to the support:

$$M(O) + C_f \rightarrow C(O) + M \quad (8)$$

In this communication we present our initial results on the preparation and characterization of such catalysts and compare the performance of catalysts prepared by ion exchange (IE) and those prepared by incipient wetness impregnation (IWI). In particular, our objective is to search for ways to enhance and control the surface migration of adsorbed oxygen; if and when achieved, this could lead to surface oxygen recombination to O_2 rather than overwhelmingly to CO_2 or CO.

From a mechanistic standpoint, combustion of VOCs catalyzed by metal oxides is of interest because analogous oxygen transfer occurs, in this case in the reverse direction: from the solid catalyst to the gas phase. Furthermore, metal oxides for controlling atmospheric pollution control have received wide attention as alternatives to supported noble metal catalysts [8], particularly hexa-aluminate and perovskite-type compounds [9,10], which have even been incorporated into the design of novel combustors [11]. Simple perovskites with the basic formula ABO_3 have been investigated extensively [12,13] for several reasons: (i) transition metal ion contribution of unusual oxidation states; (ii) the amount of non-stoichiometric oxygen; and (iii) the effect of lattice defect structures [14] on catalytic activity. In ABO_3 structures, A is a large cation and B is a small cation of the d-transition series. These oxides consist of close-packed, ordered AO_3 layers which are stacked one on top of the other and the B cations occupy all the interlayer oxygen octahedra. The stacking of an AO_3 layer in the structure may be cubic or hexagonal with respect to its two adjacent layers. The ideal structure of the perovskite-type oxide is of the cubic type [15]. When some distortions of the cubic phase are present, the cation size mismatch and cation or anion non-stoichiometry is induced. For these highly oxidative systems it is of interest to relate bulk and surface defect chemistry to catalytic activity [16].

2. Experimental

2.1. Catalyst preparation

Coal demineralization. A low-rank coal (Pecket, from southern Chile) was used as the carbon precursor. The results of its proximate analysis are listed in Table 1. The as-received particulate coal (AR-C) was ground and sieved to 53–180 μm. The size-graded coal was demineralized using the following protocol: ca. 30 g of AR-C and 200 mL of 5N HCl was magnetically stirred at 55–65 °C for 1 h and filtered. The

Table 1
Proximate analyses of as-received (AR-C) and demineralized (H-C) coals (wt.%)

	AR-C	H-C
Moisture	16.8	4.6
Ash	16.0	0.1
Volatile matter	35.3	44.8
Fixed carbon	31.9	50.5

residue was stirred in 23N HF (250 mL) at 55–65 °C for 1 h and filtered. This residue was stirred in 12N HCl (200 mL) at 55–65 °C for 1 h and filtered. The filtered coal was rinsed with boiling double-distilled water until Cl anions could not be detected (using 0.1 M $AgNO_3$ aqueous solution). The demineralized coal (H-C) was obtained after overnight drying at 100 °C in an oven. The results of proximate analysis for H-C are also listed in Table 1.

Ion exchange and impregnation. Copper, potassium, and cobalt were added to H-C by the ion-exchange (IE) method. They were also added to the demineralized coal-derived carbons by incipient wetness impregnation (IWI). The acetate salts of these metals, $Cu(Ac)_2$, KAc, and $Co(Ac)_2$, were used as catalyst precursors in both cases. For ion exchange, each H-C sample (35 g) with 300 mL of acetate aqueous solution (0.3 M for $Cu(Ac)_2$ and $Co(Ac)_2$, and 0.6 M for KAc) was magnetically stirred at 55–65 °C for 24 h. The pH of the suspension was not optimized. The slurry was filtered and washed with 2000 mL of the diluted acetate solution (0.01 M) and 500 mL of distilled water. The residual cation-exchanged coal was dried at 50 °C in a vacuum oven. These samples are denoted as Cu-C-IE, K-C-IE and Co-C-IE, respectively. The metal content was determined in all cases by atomic absorption spectroscopy. For these experiments, the samples were burnt off to remove the carbon and then dissolved in HCl. The results are summarized in Table 2. For incipient wetness impregnation, the amount of metal acetate corresponding to ca. 2 wt.% metal, dissolved in the quantity of water corresponding to the pore volume of the chars, was used; the catalysts were dried in an oven for 48 h at 30 °C and their activation was effected by exposure, for 1 h under N_2 flow, to a temperature 10 °C higher than the acetate decomposition temperature determined by thermogravimetric analysis (360.3 °C for Co, 299.4 °C for Cu and 509.9 °C for K). The corresponding designation for these samples is Cu-C-IWI, K-C-IWI and Co-C-IWI.

Coal carbonization. The cation-exchanged coal samples, as well as AR-C and H-C samples, were converted to chars at 550, 700, 850, and 1000 °C. An alumina boat-type crucible and a horizontal tubular furnace were used. The heating rate was 5 °C/min in a N_2 flow of 200 mL/min, and the final temperature was maintained for 1 h. The catalysts were obtained after cooling to 50 °C while maintaining the N_2 flow. The final heat-treatment temperature (HTT) is indicated by the last three or four digits in sample designation, e.g., Cu-C-IE-550 or Co-C-IWI-1000.

Perovskites. The perovskite-type oxides, $La_{1-x}Ca_xFeO_3$ and $La_{1-x}Ca_xNiO_3$ ($x = 0.0$, 0.2, 0.4) were prepared by the citrate method [17]. Stoichiometric amounts of an aqueous solution of the nitrates of the corresponding metals were added to an aqueous solution of citric acid with a 10% excess over the number of ionic equivalents of cations. The resulting solution was stirred for 15 min at room temperature and slowly dried at 343 K under vacuum in a rotary evaporator until gel formation was reached. The gel was then dried in an oven, slowly increasing the temperature to 523 K and maintaining it overnight to yield a solid amorphous citrate precursor. The resulting powder was crushed and sieved to obtain the desired particle size (<200 μm) and calcined at 973 K in air for 6 h.

2.2. Catalyst characterization

Both the coal-derived and the perovskite-type oxide catalysts were examined by N_2 physisorption and X-ray diffraction (XRD). Adsorption isotherms were obtained at 77 K in a volumetric apparatus (Micromeritics models ASAP 2010 and Gemini 2360). Coal-derived samples were pretreated at 150 °C and 20–30 Pa for 24 h; the perovskite-based ones were treated under N_2 at the same temperature for 2 h. The XRD spectra were obtained using Cu Kα radiation (λ = 0.1542 nm, Rigaku Geigerflex D max C).

Table 2
Metal contents in AR-C, H-C and cation-exchanged coals (wt.%)

Sample	AR-C	H-C	Cu-C-IE	K-C-IE	Co-C-IE
Na	0.23	< 0.001			
Mg	0.19	< 0.01			
Fe	0.06	0.02			
Al	2.07	< 0.01			
Ca	1.29	< 0.02			
Cu	< 0.01	< 0.01	3.65		
K	0.07	< 0.001		1.85	
Co	<0.001	< 0.001			3.35

Coal-derived catalysts were also subjected to elemental analyses: C, H, N (Leco CHN 2000) and S contents were measured directly, while metal content after coal carbonization (IE catalysts) or acetate decomposition (IWI catalysts) was determined by atomic absorption spectroscopy. They were also analyzed by thermogravimetry (TG) and differential thermal analysis (DTA) using air or N_2 flow (100 mL/min) from ambient temperature to 1000 °C at 5 °C/min (Netzsch STA 409 PC Luxx).

Perovskite-based catalysts were additionally characterized by temperature-programmed reduction (TPR, 5% H_2 in Ar, 40 cm^3/min, 10 K/min) and temperature-programmed desorption (TPD, O_2 for 1 h at 973 K, then He at 10 K/min) in a TPR/TPD 2900 Micromeritics system with a thermal conductivity detector.

2.3. Catalytic activity

Coal-derived catalysts. The reactivity of metal-loaded and metal-free chars in NO was examined in a fixed-bed flow reactor at atmospheric pressure. The catalyst sample (ca. 100 mg) was sandwiched between quartz wools and exposed to a flow of NO in He or N_2 (0.1%) at 500 mL/min. The temperature-programmed reaction (TPR) was carried out at 5 °C/min to 950 °C. The gaseous products were monitored using non-dispersive IR detectors for CO and CO_2 (Horiba PIR-2000) and a chemiluminescence analyzer for NO (Horiba CLA-220).

Perovskite-type oxides catalysts. The catalytic activity of the perovskite catalysts in the combustion of ethanol and acetyl acetate was evaluated in a conventional flow reactor at atmospheric pressure. In each experiment, 100 mg of catalyst diluted with 100 mg of inert silica was used. The reactant mixture (molar $C_4H_8O_2$:O_2:He = 1:1:98, C_2H_6O:O_2:He = 1:5:94) was fed into the reactor at 50 mL min^{-1} and the temperature was linearly increased to 423 K at 1 K min^{-1} and then maintained constant for 30 min. Reactor effluents ($C_4H_8O_2$, C_2H_6O, O_2, CO_2, H_2O) were analyzed using an on-line gas chromatograph (Hewlett Packard model HP 4890D) with a thermal conductivity detector (with a Supelco 25462 30-m capillary column). A quadrupole mass spectrometer (Shimadzu GCMS-QP 5050) was used to detect traces of products.

3. Results and discussion

3.1. NO reduction

The conventional approach to the preparation of carbon-supported catalysts is to independently produce a general-purpose activated carbon, with a maximum specific surface area and an optimum pore size distribution (which typically costs ca. \$ 2 kg^{-1}), and then to prepare the catalyst by selecting an adequate activated carbon support and devising a suitable metal loading procedure (e.g., dry mixing, atmospheric pressure or vacuum impregnation, ion exchange). While such an approach may have its advantages, here we have explored a more straightforward and in principle less expensive procedure [6], using a Chilean coal whose cost is two orders magnitude lower than that of activated carbons.

3.1.1. Catalyst behavior

The summary presented in Table 3 shows the effectiveness of the ion-exchange catalyst loading procedure. For example, with a 50% carbonization yield, 7.5% Cu might imply that close to 100% of the carboxyl groups were exchanged at the unadjusted pH of the solution, since low-rank coals are known to have up to ca. 5 mmol carboxyl groups/g [18]; however, some concomitant precipitation from the low-solubility Cu and Co acetates cannot be ruled out. The relatively low K content is thought to reflect its higher volatility and its loss from the sample during the ashing step in the elemental analysis procedure, and also presumably during catalyst heat treatment at 850 °C. In the case of IE catalysts, the BET surface area is seen to increase in the presence of metals, especially Co. (The observed 'collapse' of char porosity accessible to N_2 at 77 K upon demineralization of this low-rank coal is intriguing, and deserves further study; e.g., experiments of adsorption of CO_2 at 0 °C are in progress.) The opposite occurs for the IWI catalysts, especially for K and Cu with a BET surface area of <10 m^2/g. In Table 4 it is seen that HTT of 700 °C is optimal for the Co catalyst from the standpoint of maximizing its support surface area in both IE and IWI procedures.

Despite the relatively low BET surface areas, the XRD results (Figs. 1 and 2) suggest that, except for Cu (which exhibits sharp Cu^0 peaks), the IE and IWI catalysts may be highly dispersed, or amorphous, on the carbon surface: the most prominent features of the spectra are the broad (0 0 2) and (10) bands of the highly disordered non-graphitic coal-derived carbon at ca. 24° and 44° 2θ. The appearance of Co peaks for the higher HTT supports is also of interest: Co^0 in the higher-surface area IE catalysts and both CoO and Co^0 in the lower-surface area IWI catalysts.

The support ignition temperatures reported in Tables 3 and 4 (determined from the corresponding differential TGA curves) illustrate the high catalytic activity for the C–O_2 reaction; this is not considered to be a disadvantage, since it has been shown

Table 3
Selected properties of carbon-supported catalysts prepared at 850 °C

	H-C-850	AR-C-850	Cu-C-IE-850	K-C-IE-850	Co-C-IE-850	Cu-C-IWI-850	K-C-IWI-850	Co-C-IWI-850
Metal content (wt.%)	0.20 (Ash)	25.2 (Ash)	7.52 (Cu)	2.72 (K)	7.33 (Co)	1.53 (Cu)	1.58 (K)	1.76 (Co)
BET surface area (m^2/g)	19	185	66	21	122	8	6	15
Ignition temperature (°C)	471	388	383	316	343	423	348	477
NO reactivity[a] (°C)	811	652	674	628	612	565	713	662[b]

[a] Temperature at 10% NO conversion, for H-C and IE catalysts determined in a 12-mm reactor, and for AR-C and IWI catalysts in a 13-mm reactor.
[b] When this sample was tested in the 12-mm reactor, the temperature for 10% NO conversion was 684 °C.

Table 4
Summary of properties of carbon-supported cobalt catalysts prepared at 550–1000 °C

	Co-C-IE-550	Co-C-IE-700	Co-C-IE-850	Co-C-IE-1000	Co-C-IWI-550	Co-C-IWI-700	Co-C-IWI-850	Co-C-IWI-1000
Co content (wt.%)	6.71	7.28	7.33	7.47	1.71	1.83	1.76	1.77
BET surface area (m^2/g)	268	337	122	<10	48	69	15	16
Ignition temperature (°C)	323	303	343	441	404	446	477	495
NO reactivity[a] (°C)	482	466	610	699	610	564	684	624

[a] Temperature at 10% NO conversion, determined in a 12-mm reactor.

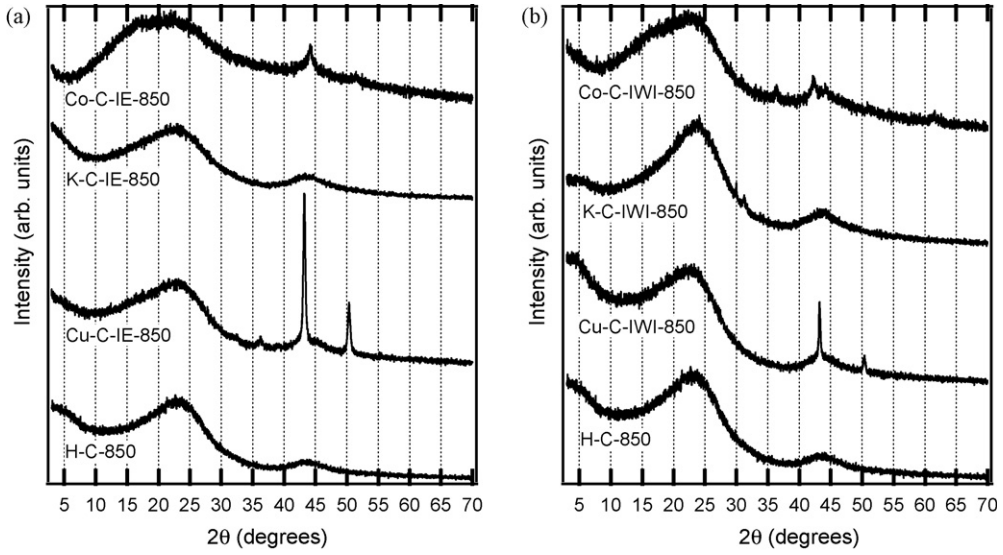

Fig. 1. XRD patterns of carbon-supported catalysts prepared at 850 °C: (a) by ion exchange (IE) and (b) by incipient wetness impregnation (IWI).

that NO reduction with carbon-supported catalysts is promoted in the presence of concomitant carbon oxidation [19] and the double role of catalyst support and reducing agent is not a liability for the inexpensive coal char [6]. For IE catalysts, the order of activity is K ≫ Co > Cu. For IWI catalysts, it is K > Cu > Co; the absence of a catalytic effect of Co (477 °C versus 471 °C for H-C-850) may be due to the dominant presence of CoO, rather than Co on the support surface (see Fig. 1b). In the case of Co-IE catalysts (Table 4), it is interesting to note that the optimum HTT (for highest catalytic activity) is 700 °C, while for Co-IWI the ignition temperature increases with HTT; the latter trend is the intuitively expected one when

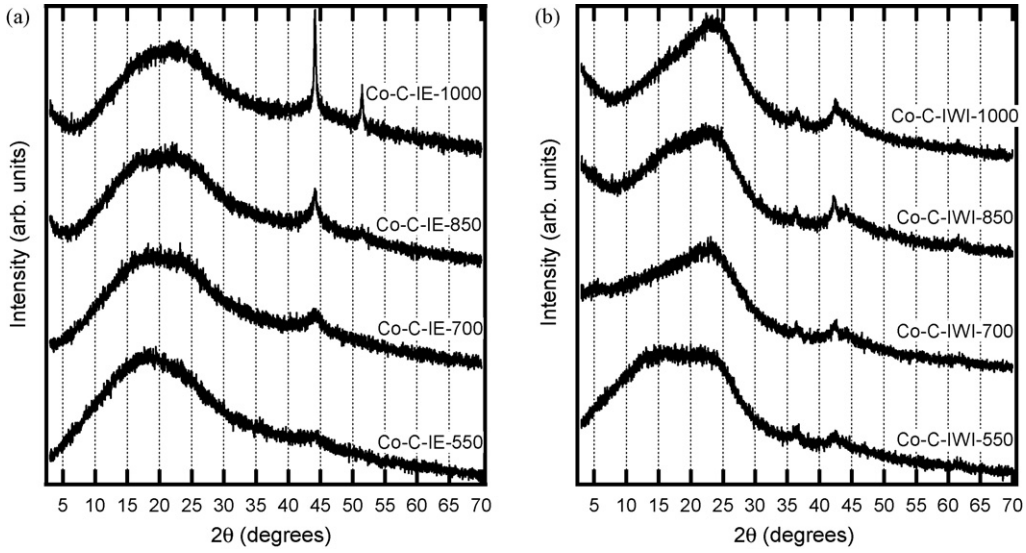

Fig. 2. XRD patterns of carbon-supported cobalt catalysts prepared by ion exchange (a) and by incipient wetness impregnation (b) at temperatures between 550 and 1000 °C.

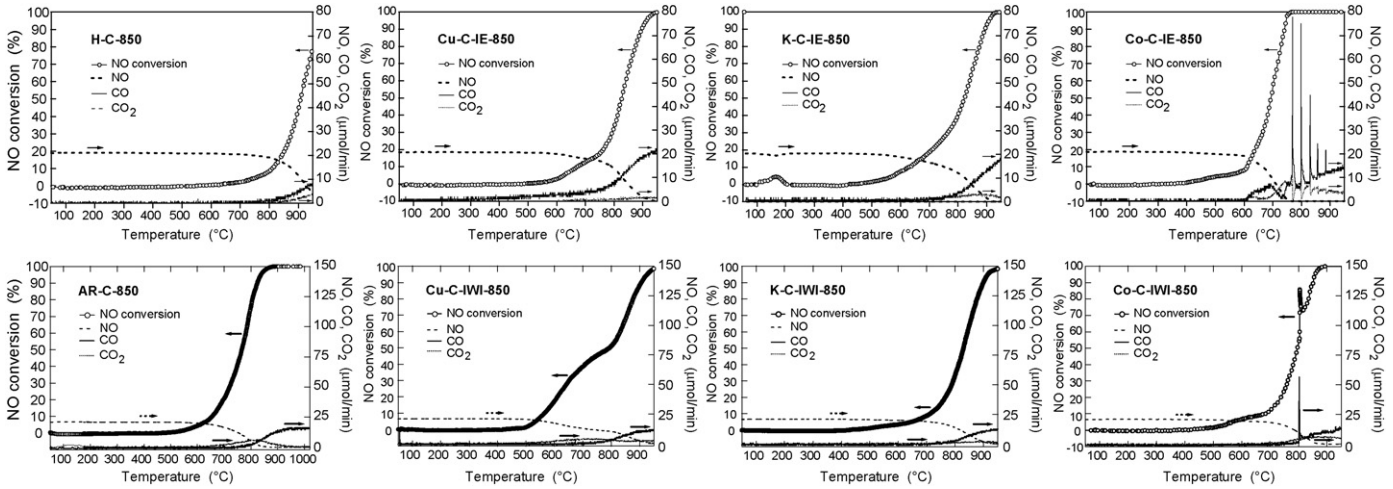

Fig. 3. Comparisons of NO reduction behavior of carbon-supported catalysts prepared at 850 °C.

metal–support interactions are important (see Section 3.1.2), while the former correlates with the BET surface area and not with either metal content or metal dispersion (at least as measured by XRD peak width). Fig. 2a does show that in the case of IE catalysts and above 700 °C there is dominant formation of Co^0, and the observed crystallite growth is consistent with the decrease in catalytic activity reported in Table 4. In the case of Co-IWI catalysts, Fig. 2b shows that there are no drastic differences in the crystallite size of the cobalt species, despite the fact that they were deposited over support surfaces (see Table 4) whose BET areas differ by a factor of 4; this is attributed to the fact that all Co-IWI catalysts were exposed to the same temperature (370 °C) to decompose the acetate.

Figs. 3 and 4, as well as Tables 3 and 4, show that the catalytic activity for NO reduction is lower than that exhibited for the C–O_2 reaction. Whether this is a consequence of less efficient oxygen transfer from the gas phase to the catalyst surface or to some of the subsequent mechanistic steps (see Eqs. (3) and (5)), which are considered to be common to both reactions [5], remains to be unraveled (see also Section 3.1.2). The relative effectiveness of the catalysts is essentially the same (when taking into account the much lower K content) for the IE series. Significant differences are observed for the IWI series, both with regard to catalyst effectiveness and support HTT. Thus, for example, K appears to be most effective for the C–O_2 reaction and Cu for NO reduction; and for NO reduction the optimum HTT was 700 °C for both Co-IE and Co-IWI, in agreement with the trends in support BET surface area.

The CO evolution results are of particular interest. (a) It is intriguing that CO is desorbed in preference to CO_2, suggesting (see Eq. (5)) a relatively low oxygen surface coverage. (b) The appearance of smaller amounts of CO_2 at the higher temperatures is also intriguing. (c) In the case of Cu, CO evolution starts – and is maintained at a relatively low level – much earlier than in the case of the more active K and Co catalysts. (d) There are significant differences in the offset between NO disappearance and CO appearance; it is least pronounced in the case of Cu-IE and most in the case of K-IE

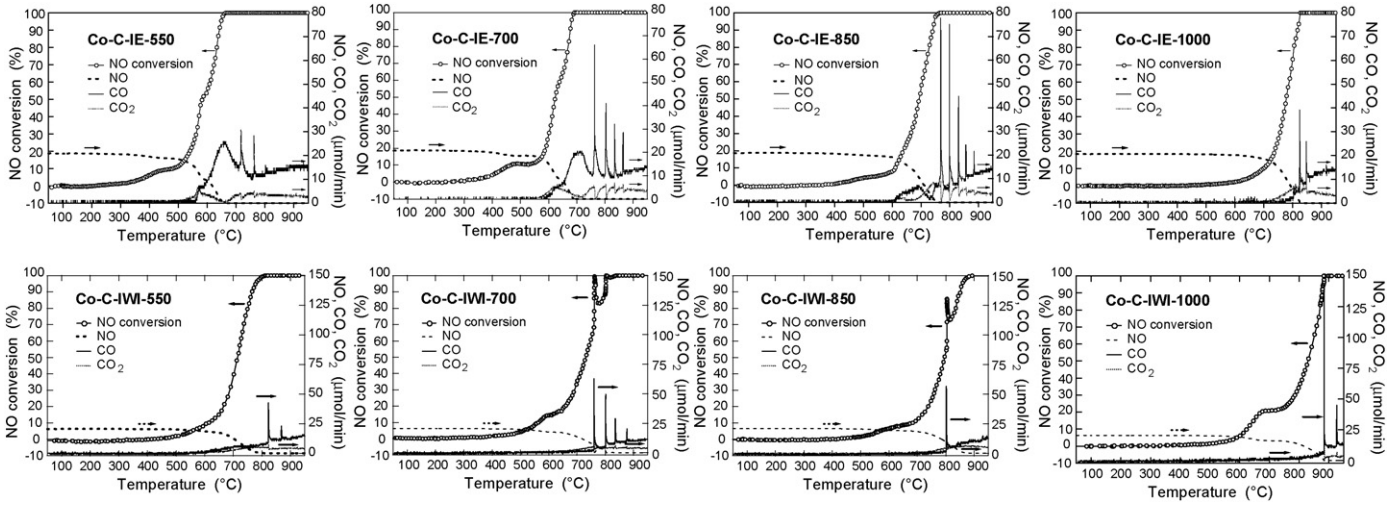

Fig. 4. Comparisons of NO reduction behavior of carbon-supported cobalt catalysts prepared at 850 °C.

catalysts. The mechanistic implications of these and other findings are analyzed next.

3.1.2. Mechanistic considerations

The essential mechanistic steps in the catalytic reaction sequence were presented in Section 1. Catalyzed oxidation of carbon, as well as NO reduction by carbon, is most often discussed in terms of oxygen transfer [4,5], at the exclusion of electron transfer [7], although electron transfer [20] is of course essential as well, if only because it determines the oxidation state of the active catalytic species. Here we address the relative importance of these steps for the two series of catalysts: (a) in the IE series both the catalyst and the support have been exposed to the same thermal treatment; (b) in the IWI series the carbon support has been prepared at temperatures varying from 550 to 1000 °C, whereas on all these supports the Cu, Co and K catalysts were exposed to 310, 370 and 520 °C, respectively.

If a mechanistic step involving the support were rate-determining, then increasing support HTT would result in monotonically decreasing catalytic (re)activity [4,6]. This was the case for the Co-IWI catalysts in the C–O_2 reaction, but not in NO reduction. Increasing support HTT in the case of Co-IE catalysts is expected to have two additional effects: decreasing catalyst dispersion and increasing extent of reduction of the catalytically active species. The fact that the Co activity order was $700 > 550 > 850 \gg 1000$ for the C–O_2 reaction and $700 > 550 \gg 850 > 1000$ for NO reduction suggests a more complex interplay among the adsorption, surface reaction and desorption steps, and this requires further study. A more detailed analysis of the XRD results may offer some clues: the low-angle portion of the spectrum ($<25^\circ$ 2θ) is consistently different for Co catalysts (see Figs. 2a and b, as well as 1a and b). In addition to possibly subtle microporosity changes evidenced in the small-angle region ($<5^\circ$ 2θ) – which are shared by some of the Cu and K catalysts – the pronounced hump centered at ca. 17° 2θ may reveal evidence of significant chemical and structural differences.

The oscillatory behavior at the higher temperatures is observed only, and consistently so, in the case of Co catalysts and it is shown in more detail in Fig. 4. As the reaction temperature increases, the CO and CO_2 peaks decrease; this is confirmed by an oxygen mass balance, which also shows that in each pulse more oxygen evolves as CO than as CO_2. And as the sample HTT increases, the intensity of the peaks exhibits a maximum. Because of the opposite slopes of CO and CO_2 evolution at this stage of the reaction, the obvious possible explanation is the Co-catalyzed carbon gasification by CO_2. It is well known that transition metals lose their catalytic activity when oxidized [7]. Therefore, the intriguing (and indeed dramatic!) results shown in Figs. 3 and 4 are thought to be the net effect of the following three reactions:

$$C + CO_2 \leftrightarrow 2CO$$

$$Co + CO_2 \leftrightarrow CoO + CO$$

$$CoO + C \leftrightarrow Co + CO$$

A confirmation of this proposal and the implications of these results for the design of more effective coal-based NO reduction catalysts are the subject of our ongoing research. A comparison of Cu-IWI-850, Co-IWI-850 and K-IWI-850 catalysts (Fig. 3) is expected to contain important clues: the least effective K catalyst is seen to be able to sustain the redox cycle (Eqs. (1)–(8)) at all temperatures, in agreement with its highest oxidation potential (2.92 V for K/K^+); in contrast, the most active Cu catalyst – with its lowest oxidation potential (-0.52 V for Cu/Cu^+ and -0.34 V for Cu/Cu^{2+}) – appears not to be able to do the same at the lowest temperature, ca. 750 °C; and the Co catalyst, with its intermediate oxidation potential (0.280 V for Co/Co^{2+}) exhibits the intriguing oscillatory behavior at intermediate temperatures.

3.2. VOC combustion

The surface areas of the perovskite catalysts, summarized in Table 5, illustrate the beneficial effect of calcium substitution, especially for the $La_{1-x}Ca_xFeO_3$ series. The corresponding XRD patterns in Fig. 5 show sharp reflections located at the expected 2θ values, thus confirming that the perovskite structure was indeed obtained after calcination of the solids at 973 K. Very orthorhombic $LaFeO_3$ (JC-PDF 37-1493) and rhombohedral $LaNiO_3$ (JC-PDF 33-0711) perovskite structures are obtained, with absence of any other crystalline phases [21,22]. Changes induced by calcium substitution can also be observed. Thus, as the degree of Ca substitution increases there is a definite shift towards larger 2θ angles, corresponding to lattice contraction [23,24], which is evidence for the substitution of lanthanum by calcium and the preservation of perovskite structure with slight distortion.

The results of TPD experiments provide information about the redox properties of the perovskites [25]. A common feature of the O_2 profiles shown in Fig. 6 is the evidence of a desorption peak centered at ca. 350 K, which originates from weakly bound oxygen species. A second peak, at ca. 500 K – which appears as a shoulder for the pure $LaFeO_3$ and $LaNiO_3$ perovskites – is attributed to the so-called α-oxygen, and has been previously reported for other substituted perovskites [26]; it is related to the substitution of calcium in the perovskite because it becomes more prominent and shifts towards higher temperatures as x increases. The last TPD signal appears above

Table 5
Summary of properties and catalytic activities of perovskite catalysts

	S_{BET} ($m^2\ g^{-1}$)	T_{50} (K)		Reaction rate ($mol\ g^{-1}\ s^{-1} \times 10^5$)	
		Ethanol	Acetyl acetate	Ethanol 473 K	Acetyl acetate 523 K
$LaFeO_3$	19.5	520	613	0.7	0.7
$La_{0.8}Ca_{0.2}FeO_3$	28.6	512	593	2.1	4.3
$La_{0.6}Ca_{0.4}FeO_3$	31.2	515	587	1.9	5.2
$LaNiO_3$	8.3	523	573	4.5	3.0
$La_{0.8}Ca_{0.2}NiO_3$	11.4	520	580	4.5	2.9
$La_{0.6}Ca_{0.4}NiO_3$	14.7	521	579	4.8	2.7

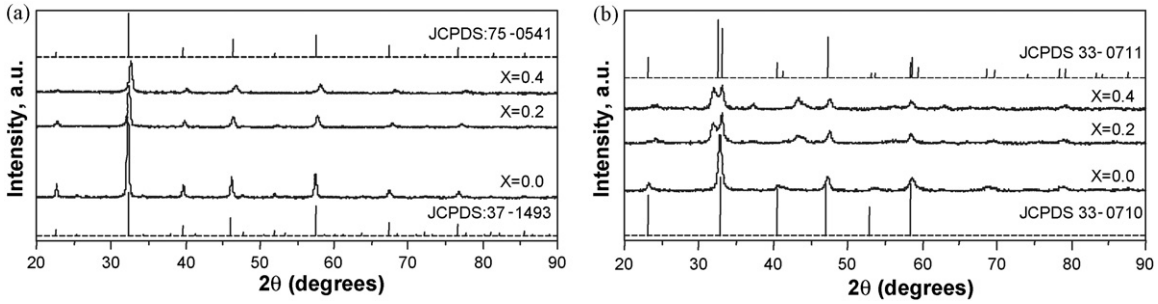

Fig. 5. X-ray diffraction patterns of perovskite-type oxide catalysts: (a) $La_{1-x}Ca_xFeO_3$ and (b) $La_{1-x}Ca_xNiO_3$.

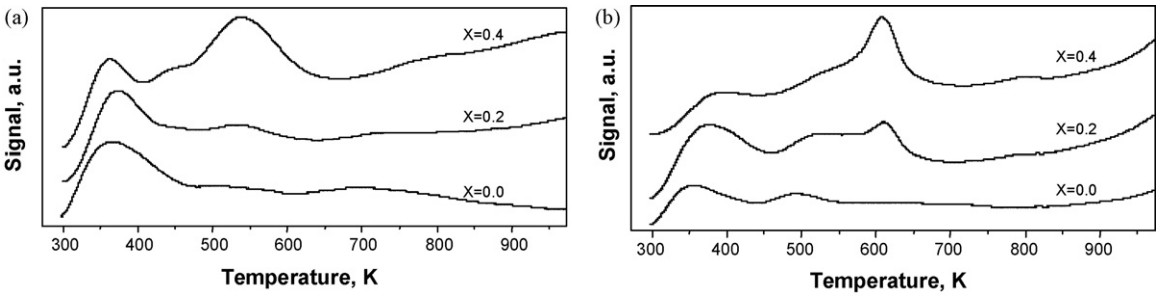

Fig. 6. Oxygen temperature-programmed desorption profiles of perovskite-type oxide catalysts: (a) $La_{1-x}Ca_xFeO_3$ and (b) $La_{1-x}Ca_xNiO_3$.

800 K and corresponds to the so-called β-oxygen, which is associated with lattice oxygen [27] and can thus be related to the redox properties of the perovskite. This feature is seen to be more prominent for the more substituted perovskites and thus corresponds to oxygen species occupying the inner vacancies created by substitution of calcium by lanthanum. Mass spectrometric analysis of the evolved gas in TPD confirms that O_2 is the only desorbed product. Therefore, the main differences in both intensity and temperature of gas evolution are linked with α-oxygen.

The TPR experiments were performed with the aim to study the reducibility of the prepared perovskites, which is a key parameter for assessing the effect of calcium addition on the stabilization of the perovskite structure. The profiles shown in Fig. 7 provide evidence for different behaviors of the two unsubstituted perovskites: while $LaFeO_3$ shows no prominent peaks, $LaNiO_3$ shows two well defined reduction peaks. The substituted $La_{1-x}Ca_xFeO_3$ perovskites show two distinct peaks, the larger at 550 K with a slight shift to higher temperatures as the degree of calcium substitution increases, followed by a broader one at 620 K (which is not clearly seen in these compressed profiles). This behavior is thought to be a consequence of cation exchange: as Ca^{2+} is exchanged by La^{3+} in the perovskite lattice, oxidation of Fe^{3+} to Fe^{4+} is necessary to compensate the lower charge of Ca^{2+} [28]. At higher temperatures, hydrogen consumption increases linearly with temperature and no maximum could be detected up to 973 K. As was mentioned previously, the presence of Fe^{4+}–Fe^{3+} couples in the substituted perovskites allows the partial reduction to Fe^{3+} which may occur in two steps, as suggested by Ciambelli et al. [29]. With regard to the $La_{1-x}Ca_xNiO_3$ series, their TPR profiles clearly reveal different intensities in the two H_2 consumption peaks, reflecting the effects of Ca substitution. Hydrogen consumption for the first peak is consistent with the reduction of Ni^{3+} to Ni^{2+}, yielding a $La_2Ni_2O_5$ phase that obviously implies oxygen loss from the structure [22]. The second peak, with a maximum consumption of H_2 at ca. 760 K for $x = 0.0$, and ca. 870 K for $x = 0.4$, is interpreted as evidence for the formation of metallic nickel deposited on lanthanum oxide, as has been reported previously [30]; its absence for $x = 0.2$ is thought to be due to the high metal dispersion or absence of its segregation.

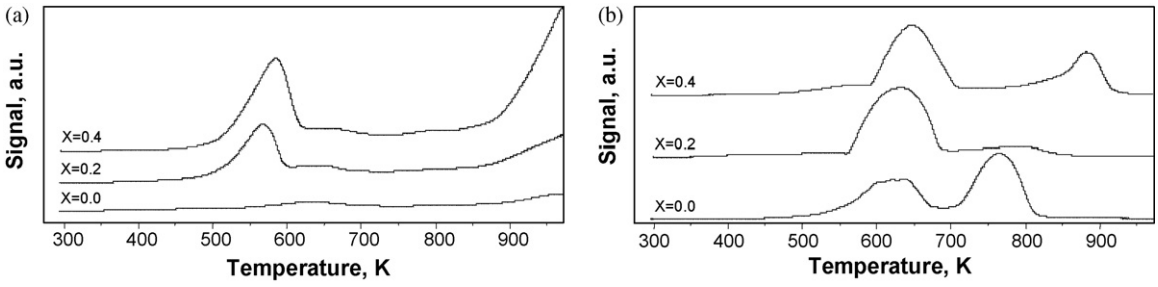

Fig. 7. Temperature-programmed reduction profiles of perovskite-type oxide catalysts: (a) $La_{1-x}Ca_xFeO_3$ and (b) $La_{1-x}Ca_xNiO_3$.

All the perovskites were tested for combustion of ethanol and acetyl acetate in a flow reactor under an excess of oxygen. Carbon dioxide and water were the only observed products for ethanol combustion, while traces of acetaldehyde were detected in acetyl acetate combustion, regardless of the degree of calcium substitution. In no case was CO observed.

The observed catalytic activity was conveniently quantified in terms of the ignition temperature (T_{50}), defined as the temperature required to obtain 50% conversion. An intrinsic activity was also determined, expressed as moles converted per second and gram of catalyst at 473 K for ethanol and 523 K for acetyl acetate. The results are compiled in Table 5. For the $La_{1-x}Ca_xFeO_3$ series, a decrease in the ignition temperature as a function of substitution degree is observed, whereas an increase is observed with the $La_{1-x}Ca_xNiO_3$ series. In addition, with the $La_{1-x}Ca_xFeO_3$ perovskites a different trend was observed for acetyl acetate versus ethanol combustion: a continuous decrease in ignition temperature (or increase in the reaction rate) for the former with increasing substitution degree, compared to a larger initial decrease in T_{50} followed by saturation for the latter reaction. In an attempt to clarify these trends, the intrinsic activity of the samples was calculated at steady state and these results are also summarized in Table 5. In ethanol combustion the activity is seen not to depend on nickel content. Such behavior has been observed mainly in combustion of polar molecules [31]. In contrast, the activity for acetyl acetate combustion increases as the degree of substitution increases, in parallel with the presence of α-oxygen. Thus, the proposed reaction mechanism is an oxidation–reduction cycle of the Mars-van Krevelen type [32] combined with a Rideal adsorption step.

4. Conclusions

Our initial study of coal-based NO reduction catalysts, with relatively low metal loadings, has not yet resulted in the development of very active catalysts, but it has shown us the direction for further improvements and has revealed some intriguing phenomena, especially with regard to differences between catalysts prepared by ion exchange and incipient wetness impregnation and the effects of heat treatment of both the support and the supported catalysts on the various mechanistic (redox) steps. An intermediate support activation step, to increase the surface area and thus allow higher metal loadings without dispersion loss, may be necessary.

The results obtained for the perovskite catalysts show that an increasing substitution of calcium by lanthanum in the $La_{1-x}Ca_xFeO_3$ series is beneficial for VOC catalytic combustion; the electronic perturbation is compensated by an oxidation state increase of part of Fe^{3+} to Fe^{4+}. In contrast, the analogous substitution has no effect on catalytic activity for the $La_{1-x}Ca_xNiO_3$ series; for these perovskites the electronic perturbation cannot be compensated by nickel ions and thus a change in the crystalline structure and segregation of NiO crystallites occurs, resulting in a non-stoichiometric perovskite plus nickel oxide. These findings are consistent with a combined Rideal/Mars-van Krevelen redox mechanism.

Acknowledgments

This ‘‘South American connection’’ of Al Vannice goes a long way back. In the early 1980s, one of the senior authors (LRR) went from an entry teaching position at the University of Concepción to spend a postdoctoral year in Al’s lab at Penn State. In the mid-1990s, partly upon recommendation of LRR and his Chilean wife, Al and Bette Ann visited Concepción and had a busy agenda: Al discussed research with various catalysis groups from Concepción and Talca, and of course took time to visit the local antique car dealers; Bette Ann enjoyed shopping ceramic art objects at the local mall and exchanging views about teaching English with GP’s sister; and both of them enjoyed the local food and especially wine while dining with GP, Patricio Reyes and their colleagues. Al was back here again in May 2001, as an invited professor for the Millennium Nucleus project (ICM P99-92), and he gave a short course on selective hydrogenation catalysts. We thank Al and Bette Ann for their support and friendship and wish Al an enjoyable retirement, with many miles on the road and in the air to visit again their colleagues and friends all over the world. This study was carried out in the framework of projects 1060702 and 1060950 of FONDECYT-Chile. One of the authors (SU) gratefully acknowledges the postdoctoral fellowship granted by the MECESUP-Chile program, project UCO0108.

References

[1] L.R. Radovic, F. Rodríguez-Reinoso, in: P.A. Thrower (Ed.), Chemistry and Physics of Carbon, vol. 25, Marcel Dekker, New York, 1997, pp. 243–358.
[2] C.A. León y León, L.R. Radovic, in: P.A. Thrower (Ed.), Chemistry and Physics of Carbon, vol. 24, Marcel Dekker, New York, 1994, pp. 213–310.
[3] A. Damjanovic, M.A. Genshaw, J.O.M. Bockris, J. Electrochem. Soc. 114 (1967) 1107.
[4] L.R. Radovic, in: K.H.J. Buschow, et al. (Eds.), Encyclopedia of Materials: Science and Technology, Pergamon Press, Oxford, 2001, pp. 975–985.
[5] M.J. Illán-Gómez, A. Linares-Solano, L.R. Radovic, C. Salinas-Martínez de Lecea, Energy Fuels 10 (1996) 158.
[6] M.J. Illán-Gómez, C. Salinas-Martínez de Lecea, A. Linares-Solano, L.R. Radovic, Energy Fuels 12 (1998) 1256.
[7] P.L. Walker Jr., M. Shelef, R.A. Anderson, in: P.L. Walker, Jr. (Ed.), Chemistry and Physics of Carbon, vol. 4, Marcel Dekker, New York, 1968 , pp. 287–383.
[8] G. Pecchi, P. Reyes, I. Concha, J.L.G. Fierro, J. Catal. 179 (1998) 309.
[9] M. O’Connell, A.K. Norman, C.F. Hüttermann, M.A. Morris, Catal. Today 47 (1999) 123.
[10] L.J. Tejuca, J.L.G. Fierro, Properties and Applications of Perovskite-Type Oxides, Marcel Dekker, New York, 1993.
[11] R.J.H. Voorhoeve, in: H.H. Burton, R.L. Garten (Eds.), Advanced Materials in Catalysis, Academic Press, New York, 1977, p. 127.
[12] S. Irusta, M.P. Pina, M. Meléndez, J. Santamaría, Catal. Lett. 54 (1998) 69.
[13] K. Poplawski, J. Lichtenberger, F.J. Keil, K. Schnitzlein, M.D. Amiridis, Catal. Today 62 (2000) 329.
[14] N. Yamazoe, Y. Teraoka, Catal. Today 8 (1990) 175.
[15] Z. Yu, L. Gao, S. Yuan, Y. Wu, J. Chem. Soc., Faraday Trans. 88 (1992) 3245.
[16] C.N.R. Rao, J. Gopalakrishnan, New Directions in Solid State Chemistry, Cambridge University Press, Cambridge, 1997, p. 53.
[17] P. Courty, H. Ajot, C. Marcilly, B. Delmon, Powder Technol. 7 (1973) 21.
[18] H.N.S. Schafer, Fuel 49 (1970) 271;
H.N.S. Schafer, Fuel 49 (1970) 197.

[19] H. Yamashita, H. Yamada, T. Kyotani, L.R. Radovic, A. Tomita, Energy Fuels 7 (1993) 85.
[20] F.J. Long, K.W. Sykes, Proc. Roy. Soc. A 215 (1952) 100.
[21] E. Bontempi, C. Garzella, S. Valetti, L.E. Depero, J. Eur. Ceram. Soc. 23 (2003) 2135.
[22] H. Provendier, C. Petit, C. Estournes, S. Libs, A. Kienemann, Appl. Catal. A 180 (1999) 163.
[23] K. Asai, H. Sekisawa, J. Phys. Soc. Jpn. 49 (1980) 90.
[24] A. Chainani, D.D. Sarma, I. Das, E.V. Sampathkumaran, J. Phys. Condens. Matter 8 (1996) L631.
[25] M. Imamura, N. Matsubayashi, H. Shimada, J. Phys. Chem. B 104 (2000) 7348.
[26] N.A. Merino, B.P. Barbero, P. Grange, L.E. Cadús, J. Catal. 231 (2005) 232.
[27] Z. Zhao, X. Yang, Y. Wu, Appl. Catal. B 8 (1996) 281.
[28] B.P. Barbero, J.A. Gamboa, L.E. Cadús, Appl. Catal. B 65 (2006) 21.
[29] P. Ciambelli, S. Cimino, S. De Rossi, M. Faticanti, L. Lisi, G. Minelli, I. Pettiti, P. Porta, G. Russo, M. Turco, Appl. Catal. B 24 (2000) 243.
[30] S. Kawasaki, M. Takano, Y. Takeda, Solid State Ionics 108 (1998) 221.
[31] P.N. Trikalitis, P.J. Pomonis, Appl. Catal. A 131 (1995) 309.
[32] M. Stojanovic, C.A. Mims, H. Moudallal, Y.L. Yang, A.J. Jacobson, J. Catal. 166 (1997) 324.